ENVIRONMENTAL RESEARCH
LETTERS

LETTER • OPEN ACCESS

A biogeochemical model of mineral-based ocean alkalinity enhancement: impacts on the biological pump and ocean carbon uptake

To cite this article: Mojtaba Fakhraee *et al* 2023 *Environ. Res. Lett.* **18** 044047

IOP Publishing Environ. Res. Lett. 18 (2023) 044047 https://doi.org/10.1088/1748-9326/acc9d4

ENVIRONMENTAL RESEARCH
LETTERS

OPEN ACCESS

RECEIVED
17 November 2022

REVISED
14 March 2023

ACCEPTED FOR PUBLICATION
3 April 2023

PUBLISHED
17 April 2023

LETTER

A biogeochemical model of mineral-based ocean alkalinity enhancement: impacts on the biological pump and ocean carbon uptake

Mojtaba Fakhraee[1,3], **Zijian Li**[1,3], **Noah J Planavsky**[2,*] **and Christopher T Reinhard**[1,*]

[1] School of Earth and Atmospheric Sciences, Georgia Institute of Technology, Atlanta, GA, United States of America
[2] Department of Earth and Planetary Sciences, Yale University, New Haven, CT, United States of America
[3] These authors contributed equally to this work.
[*] Authors to whom any correspondence should be addressed.

E-mail: chris.reinhard@eas.gatech.edu and noah.planavsky@yale.edu

Keywords: carbon dioxide removal, climate mitigation, ocean alkalinity enhancement

Supplementary material for this article is available online

Abstract

Minimizing anthropogenic climate disruption in the coming century will likely require carbon dioxide removal (CDR) from Earth's atmosphere in addition to deep and rapid cuts to greenhouse gas emissions. Ocean alkalinity enhancement—the modification of surface ocean chemistry to drive marine uptake of atmospheric CO_2—is seen as a potentially significant component of ocean-based CDR portfolios. However, there has been limited mechanistic exploration of the large-scale CDR potential of mineral-based ocean alkalinity enhancement, potential bottlenecks in alkalinity release, and the biophysical impacts of alkaline mineral feedstocks on marine ecology and the marine biological carbon pump. Here we a series of biogeochemical models to evaluate the gross CDR potential and environmental impacts of ocean alkalinity enhancement using solid mineral feedstocks. We find that natural alkalinity sources—basalt and olivine—lead to very low CDR efficiency while strongly perturbing marine food quality and fecal pellet production by marine zooplankton. Artificial alkalinity sources—the synthetic metal oxides MgO and CaO—are potentially capable of significant CDR with reduced environmental impact, but their deployment at scale faces major challenges associated with substrate limitation and process CO_2 emissions during feedstock production. Taken together, our results highlight distinct challenges for ocean alkalinity enhancement as a CDR strategy and indicate that mineral-based ocean alkalinity enhancement should be pursued with caution.

Carbon dioxide removal (CDR) from Earth's atmosphere is likely to play a significant role in mitigating anthropogenic climate disruption over the coming decades, with active CDR likely to be an essential part of achieving key climate thresholds even with deep and rapid cuts to anthropogenic greenhouse gas emissions [1–3]. A wide range of CDR approaches is currently under consideration [4, 5], but these vary considerably in how rapidly they could be deployed at scale and in the level of certainty surrounding potential risks and co-benefits. One approach that has remained largely at the concept stage is 'ocean alkalinity enhancement'—manipulating marine carbonate chemistry to foster more rapid uptake of atmospheric CO_2 into the surface ocean. This approach has garnered significant recent interest [5], in part due to the vast carbon storage potential of Earth's oceans [6, 7], and could in principle be achieved a variety of ways [8–13]. The most widely discussed technique is the dissolution of alkaline mineral feedstocks in the surface ocean, including olivine (Mg_2SiO_4) and alkaline metal oxides (MgO, CaO). When these phases dissolve in the mixed layer of the ocean they create a pulse of alkalinity that can both counteract anthropogenic acidification of surface oceans and potentially drive enhanced uptake of anthropogenic CO_2 from the atmosphere into the ocean.

Although there have been important steps forward in understanding the regional and global impacts of idealized alkalinity addition to surface oceans [10, 14–19], there are at present no estimates of the CDR potential and environmental impacts of mineral-based ocean alkalinity enhancement that are grounded in marine particle dynamics. Specifically, although previous work has sought to explore the impacts of imposed dissolved alkalinity fluxes to the surface ocean or has inverted prescribed atmospheric pCO_2 trajectories for required surface ocean alkalinity fluxes, no previous work has mechanistically modeled the dynamics of alkalinity release from potential mineral feedstocks as they interact with the marine particle factory—the complex set of physical and chemical processes that control the aggregation, disaggregation, and settling of marine particles in the ocean. In addition, there has been limited exploration of the potential biophysical impacts of alkaline mineral feedstocks on marine ecology, the formation and recycling of marine aggregates, and the ocean's biological carbon pump. This basic knowledge gap represents a significant barrier to deployment at scale and to a productive debate on the merits and potential pitfalls of carbon capture through mineral-based ocean alkalinity enhancement.

Here we present a new biogeochemical model of marine particle cycling designed specifically to interrogate the impacts and carbon capture potential of adding alkaline mineral feedstocks to the surface oceans as a CDR strategy. To our knowledge, this is the first attempt to simulate ocean alkalinity production from natural and synthetic mineral feedstocks with a mechanistically explicit particle model and to explore the potential impacts of this process on particulate biogeochemical fluxes within the marine biological pump. We first use the model to evaluate the dissolution and potential alkalinity fluxes to the surface ocean from a range of widely discussed feedstocks for mineral-based ocean alkalinity enhancement. We then evaluate the impact of alkaline mineral feedstocks on marine particle composition and discuss the implications of this for the marine biological carbon pump and potential trophic impacts. Finally, we use the alkalinity fluxes from our particle model as a boundary condition to drive an Earth system model and use this to estimate gross CDR through ocean CO_2 uptake for a range of idealized deployment scenarios.

1. Materials and methods

1.1. A stochastic model of marine particle cycling

The stochastic particle model is a 1D (column) model of the physics and biogeochemistry of marine particles embedded in a reaction-transport framework. The constitutive element of our model, referred to here as an 'aggregate', is a cluster of primary particles that emerges through interaction between phytoplankton cells (e.g. coccolithophorids, diatoms, picoplankton), various minerals (basalt, olivine, MgO, and CaO), and terrigenous dust (figure S1, table S1). The model calculates the sinking rates and physical properties (density, porosity, size) of 10^6 aggregates at each depth, with the distribution of primary particles (minerals, dust particles, picoplankton, coccolithophorids, diatoms, etc) in each aggregate calculated according to the relative contribution flux of each primary particle to the total flux of material at each depth. This stochastic representation of particle aggregation/disaggregation, vertical sinking, and zooplankton grazing is then coupled with organic matter remineralization and temperature- and pH-dependent mineral transformation and alkalinity release to the water column. The model is based on a previously published model designed to reconstruct the geologic history of the ocean biological carbon pump [20–22], but has been extensively modified to represent mineral-based ocean alkalinity enhancement. The conceptual mechanics of the model are briefly summarized here, while all model equations, default parameters, validation against empirical observations, and sensitivity analysis can be found in tables S1–S3 and figures S2–S8.

The model calculates the probability of aggregate formation by parameterizing the collision dynamics between aggregates or primary particles as a function of Brownian motion, fluid shear, and differential settling (i.e. relatively large and more rapidly settling particles/aggregates sweeping up smaller particles/aggregates). Aggregates form with a fractal structure with a dimension, D_N, that describes its porosity ($p \sim r_a^{D_n}$, where p is the number of primary particles in the aggregate and r_a is the radius of the aggregate) [23]. The closer D_N is to 3, the more the structure fills up three-dimensional space, thus lowering its overall porosity. Aggregate sinking rates are calculated as a function of excess density relative to seawater, with drag coefficients corrected for the impact of turbulence and viscous forces based on aggregate sinking rate and the local kinematic viscosity of seawater. Model aggregates are assumed to sink vertically (i.e. there is no lateral current transport of aggregates).

Observations from the modern ocean suggest an important role for zooplankton in the marine particle cycle [24, 25]. In particular, particle ingestion and fecal pellet production by zooplankton can represent an important vertical flux of organic carbon and other particle constituents, while evidence of slow-sinking oceanic aggregates in the modern deep ocean also suggests an important role of disaggregation/fragmentation of oceanic aggregates in the marine biological pump [26], much of which may be mediated by interaction with zooplankton. The encounter rate of zooplankton with marine aggregates in the model is parameterized as a function of net primary production, consistent with observations

from the modern oceans (e.g. [19, 20]). Any discrete zooplankton-aggregate encounter event can lead to either ingestion or fragmentation, the likelihood and results of which are parameterized based on fragmentation experiments with tethered *Euphausia pacifica* [22, 27] and a power law relationship for fragment production [22]. Aggregates that are not fragmented and contain organic matter are ingested, resulting in the production of fecal pellets whose size is parameterized as a function of copepod prosome length stochastically sampled from a uniform prior distribution of prosome lengths for multiple zooplankton size classes (table S2).

The biogeochemical module of the model tracks organic matter degradation, precipitation and dissolution of calcium carbonate, and the dissolution of alkaline mineral feedstocks. Organic matter degradation in the water column follows a power law formulation in which degradation rates are a function of the amount and reactivity of organic matter [28, 29], the latter of which is a function of organic matter age, the average sinking rate of aggregates, and seawater temperature. The model also tracks the physical properties and dissolution kinetics of four alkaline mineral feedstocks: (1) crystalline basalt; (2) olivine (forsterite); (3) MgO (periclase); and (4) CaO (burnt lime). Feedstock dissolution is temperature- and pH-dependent and is parameterized for all phases using Arrhenius expressions for the key governing reactions under acidic and basic conditions (see supplementary information). Pre-exponential factors, apparent activation energies, and reaction orders are derived from fitting experimental results for each feedstock (table S3, figures S9–S12). Previous work on ocean-based enhanced weathering has ignored differences in particle size within the reacting particle pool, and instead assumes that reacting feedstock grains sink as perfect spheres with a single uniform spherical diameter (e.g. [10]). However, mechanical comminution generally produces an approximately log-normal distribution of feedstock particle sizes [30], whose modal size and dispersion will depend on initial feedstock and grinding/milling technology [31, 32]. Our default model builds from recent work on enhanced silicate weathering in agricultural systems and other terrestrial settings [32, 33], employing a particle size distribution (PSD) rather than a single feedstock particle size. By default our feedstock PSD is that of [33], discretized into the size-mass fraction bins shown in figure S13.

1.2. Earth system modelling of ocean alkalinity enhancement

We explore the impacts of large-scale ocean alkalinity enhancement using solid alkalinity sources with a 'carbon-centric' version of the Grid ENabled Integrated Earth system model—cGENIE [34, 35]. The ocean physics and climate model components of cGENIE comprise a reduced physics (frictional geostrophic) 3D ocean circulation model coupled to a 2D energy-moisture balance model and a dynamic-thermodynamic sea ice model [36, 37]. Heat, salinity, and biogeochemical tracers are transported via parameterized isoneutral diffusion and eddy-induced advection [36–38]. The ocean model exchanges heat and moisture with the atmosphere, sea ice, and land while being forced at the ocean surface by zonal and meridional wind stress according to a specified static wind field. Heat and moisture are horizontally mixed throughout the atmosphere and exchange heat and moisture with the ocean and land surfaces, with precipitation occurring above a given relative humidity threshold. The sea ice model tracks horizontal ice transport and exchanges of heat and fresh water, using the thickness, areal fraction, and concentration of ice as prognostic variables. Full descriptions of the climate model and ocean physics can be found in [36] and [37]. The ocean model is configured here as a 36×36 equal-area grid (uniform in longitude and sine of latitude) with 16 logarithmically spaced depth levels and seasonal forcing at the ocean surface.

The ocean biogeochemistry module in cGENIE controls air-sea gas exchange and the transformation and repartitioning of biogeochemical tracers within the ocean. The ocean biological carbon pump is driven by a parameterized uptake rate of nutrients in the surface ocean, with this flux converted stoichiometrically to biomass that is then partitioned into particulate or dissolved organic matter for downstream advective transport, sinking, and remineralization within the ocean interior. Dissolved organic matter is transported with the ocean circulation and decays according to a specified time constant, while particulate organic matter is instantaneously exported from the surface ocean and is remineralized within the ocean interior following an exponential decay function with a specified remineralization length scale. The ocean biogeochemistry also contains a fully coupled carbonate system, which tracks individual dissolved inorganic carbon species, dissolved alkalinity, and ocean pH. Calcium carbonate forms in surface ocean grid cells at a stoichiometric ratio with organic matter production and is dissolved in the ocean interior or shallow marine sediments depending on ambient temperature, pressure, and carbonate chemistry [39]. Detailed description and validation of biogeochemistry in cGENIE is provided in [35, 40].

The model climate system and carbonate cycle are spun up as a closed system for 20 kyr with atmospheric abundances of CO_2, CH_4, and N_2O imposed at preindustrial values in order to bring the ocean-atmosphere system and shallow sediments into steady state. All subsequent simulations are branched from the spinup at model year 1765, and run to year 2300 according to the representative concentration pathway (RCP) and extended concentration pathway (ECP) scenarios for atmospheric CO_2, CH_4, and N_2O

[41]. Time-varying atmospheric abundances of CH_4 and N_2O are imposed according to a given RCP/ECP trajectory for all simulations, while atmospheric CO_2 abundance is emission-driven. The emission trajectory for a given RCP is first computed by the model by prescribing the atmospheric CO_2 trajectory for that scenario, with all subsequent runs utilizing the emission trajectory diagnosed in cGENIE for each RCP/ECP pathway. Concentration-driven and inverted emission-driven atmospheric compositions are shown in figure S19. Temperature trajectories are compared to CMIP5 results in figure S20 for the moderate-emissions (RCP4.5) and high-emissions (RCP8.5) pathways, while surface ocean carbonate system parameters are compared to gridded observational data in figure S21.

We use the particle model to compute the depth-integrated alkalinity release during CaO dissolution within the upper 80 m of a coastal marine water column at three different application rates referred to here as 'low' (100 g m^{-2} y^{-1}), 'moderate' (300 g m^{-2} y^{-1}), and 'high' (500 g m^{-2} y^{-1}) application scenarios. This depth range corresponds to the upper grid cell resolution in the cGENIE ocean model but is also a reasonable annually averaged value for much of the global ocean [42]. The computed alkalinity fluxes are introduced as dissolved tracer fluxes into surface ocean grid cells (e.g. as dissolved Ca^{2+} and alkalinity) starting at year 2030 according to two different idealized deployment scenarios (figure S22). In the first, alkalinity enhancement is deployed exclusively along coastlines within 60°N/S, while in the second the same overall mass flux is spread across regions of relatively high background sea-air gas exchange fluxes of CO_2. Results from the 'coastal' scenario are discussed in the Main Text, while results from the 'degas' scenario are shown in figures S23 and S24. We quantify CDR as the time-varying difference in the globally integrated air-sea flux of CO_2 between a control simulation and a simulation including ocean alkalinity enhancement.

A full techno-economic assessment across a range of deployment strategies will ultimately be required to establish plausible feedstock application rates for this carbon management approach. However, we can estimate the overall mass fluxes implied by our deployment scenarios by combining the area-normalized feedstock flues implemented in our particle model with the deployment areas in the two idealized scenarios (which are set equal by design). The overall mass (feedstock) fluxes implied by our low, moderate, and high application scenarios are 6.2, 18.6, and 31.1 Gt of feedstock per year, respectively (figure S25). This corresponds respectively to 10.3, 31.0, and 51.8% of current (2020) raw mineral (non-metallic) and ore use [43], and to 5.6, 16.9, and 28.3% of estimated raw mineral and ore use in 2060 [44]. For comparison, current global cement production is ~4 Gt y^{-1} [45] and has been projected to roughly double by 2100 [46, 47], while global available carbonate mineral deposits shallower than 25 m and within 50 km of coastlines amount to ~570 Gt y^{-1} of raw feedstock potential if deployed between 2030 and 2100 [48].

2. Results and discussion

2.1. Mineral-based ocean alkalinity enhancement and the marine biological pump

Natural silicate feedstocks (olivine and/or basalt) are rapidly removed from the surface ocean via marine particles relative to dissolution kinetics, dramatically attenuating water column dissolution at shallow depths (figure 1(A)). For example, the near-surface effectiveness of alkalinity release (defined here as the alkalinity release relative to complete dissolution within the upper 80 m of the water column) is well below 10% for basalt feedstock, regardless of feedstock application rate (figure 1(B)). Surface alkalinity release from olivine is more significant and increases as a function of feedstock application rate (figure 1(B)). However, even at high application rates and very small grain sizes (see supplementary information), the effectiveness of alkalinity release from olivine is limited.

In contrast, both MgO and CaO show very rapid near-surface dissolution, with depth-integrated alkalinity release in the upper 80 m approaching ideal stoichiometric release of feedstock alkalinity (figures 1(A) and (B)). Integrated alkalinity release shows a slight dependence on feedstock application rate for MgO, while alkalinity production from CaO is essentially complete within the upper portion of the ocean mixed layer regardless of application rate—making its behavior similar to a more direct alkalinity source such as NaOH (figure 1(B)). These results indicate that for vast regions of the coastal and open oceans natural basalt and olivine will be relatively ineffective at producing near-surface alkalinity and carbon capture from the atmosphere, while alkaline metal oxides should promote atmospheric CO_2 uptake even in regions with relatively shallow mixed layer depths. The possible exception to this dichotomy may be Mg-based phases (e.g. both MgO and brucite, $Mg(OH)_2$, which should behave similarly in the surface ocean; see supplementary information), the dissolution of which can be rapid but for which depth-integrated alkalinity release and impacts on the biological pump will depend on local net primary productivity and feedstock application rate (see below; figures S16–18).

Our model predicts that application of crushed olivine and natural basalt will have a significant impact on the organic content of marine aggregates and rates of feeding and fecal pellet production in marine zooplankton (figure 2). The average organic content of marine particles drops by over an order of magnitude with olivine/basalt application, even

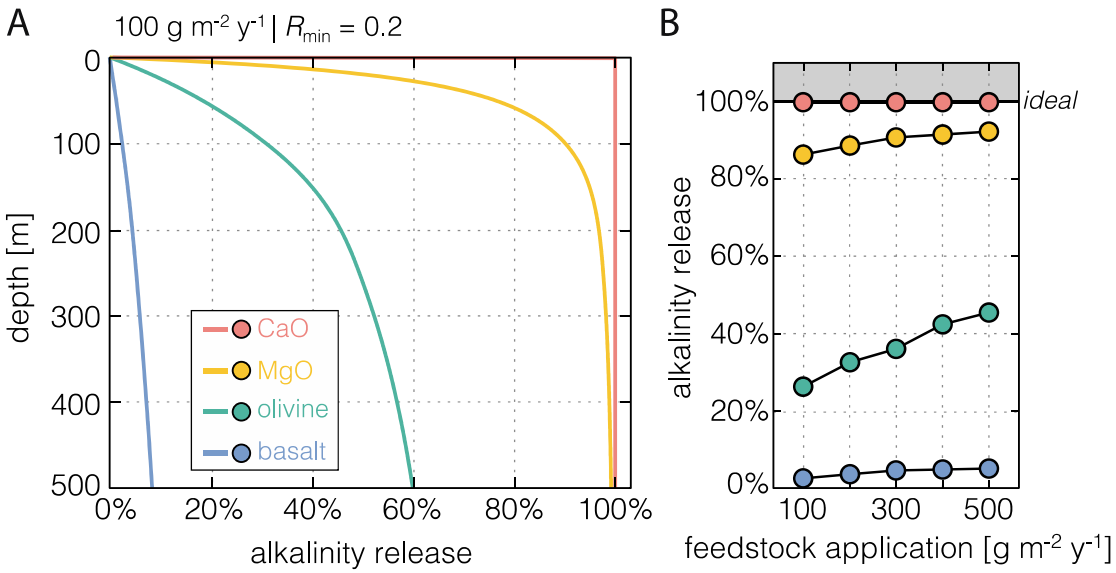

Figure 1. Water column alkalinity release from solid feedstocks in the particle model. (A) Relative alkalinity release (which fosters carbon capture) as a function of depth for natural basalt, olivine, magnesium oxide (MgO), and calcium oxide (CaO). Results are shown for an idealized coastal marine ecosystem with a feedstock application rate of 100 gC m^{-2} y^{-1} and a ratio between feedstock application rate and net primary productivity (R_{min}) of 0.2 (g/g). (B) Depth-integrated efficiency of alkalinity release in the upper 80 m as a function of feedstock application rate. The grey shaded box denotes ideal (complete) alkalinity release in the surface ocean.

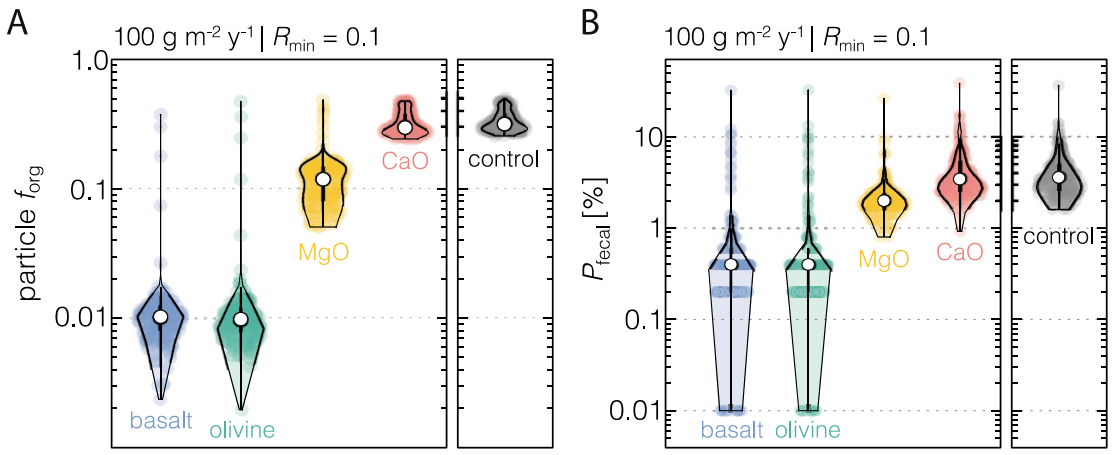

Figure 2. Impact of solid alkalinity sources on marine particle composition and zooplankton grazing in the particle model. (A) Values of average particle organic matter fraction (f_{org}) across all particles formed in the stochastic model within the upper 200 m, an operative depth range for a number of economically important fish species [68] (see also figure S13), compared to those of a control simulation with no feedstock addition. Open circles show median values, while violin plots show the distribution of results across all depths within the upper ocean. Results are shown for an idealized coastal marine ecosystem with a feedstock application rate of 100 gC m^{-2} y^{-1} and a ratio between feedstock application rate and net primary productivity (R_{min}) of 0.1 (g/g). (B) Values of zooplankton fecal pellet production within the upper 200 m of the water column compared to those of a control simulation with no feedstock addition. Fecal pellet production is given as the percentage of zooplankton encounter events with potential food particles that lead to particle ingestion and fecal pellet production (P_{fecal}).

at relatively low application rates (figure 2(A)). This decrease in food quality, which is driven by a decrease in the relative organic matter content of aggregates at the expense of slowly dissolving minerals, leads in turn to a significant drop in zooplankton feeding and fecal pellet production (figure 2(B)).

These results have significant implications for the biological carbon pump and surface marine ecosystems. The packaging of particulate organic carbon in zooplankton fecal pellets represents an important transfer mechanism for carbon into the ocean interior [25, 49, 50], with potentially cascading impacts on marine nutrient abundance and dissolved oxygen availability linked with changes to spatial patterns of nutrient release and oxygen consumption during organic matter remineralization. In addition, because zooplankton is a key food source for larval fish and planktonic crustaceans significant changes to zooplankton food quality and grazing efficiency would be expected to induce

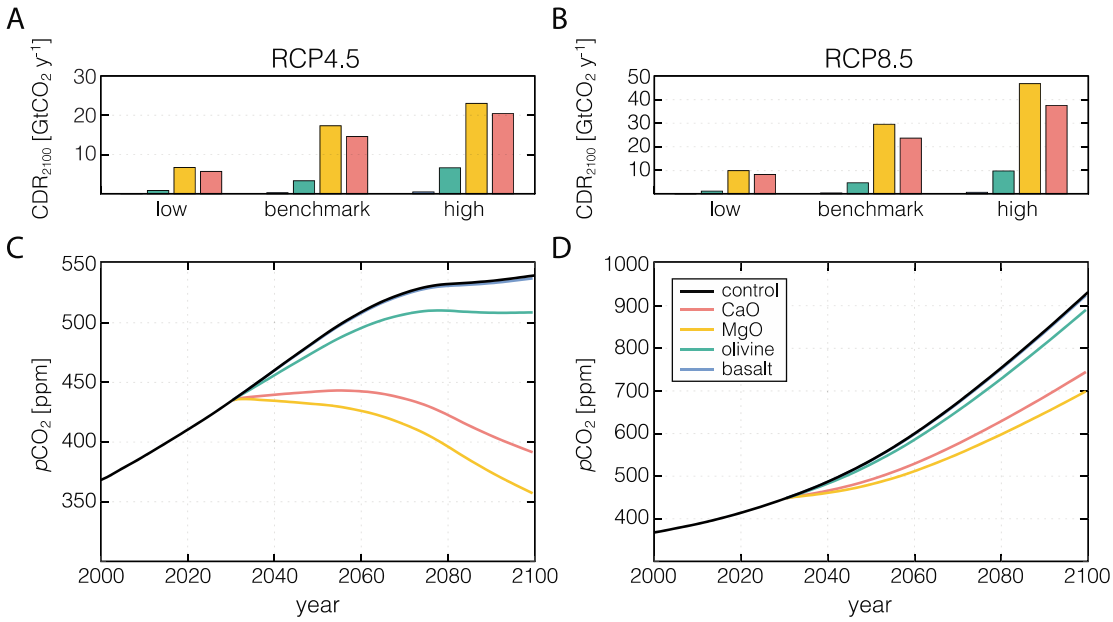

Figure 3. Gross carbon dioxide removal (CDR) during ocean alkalinity enhancement in an Earth system model. Results are shown for a moderate-emissions pathway (RCP4.5; A, C) and a high-emissions pathway (RCP8.5; B, D), with feedstock application along coastlines between 60° N/S latitude (see supplementary information). Ocean alkalinity enhancement begins in year 2030. (A), (B) Rates of carbon dioxide removal in model year 2100 (CDR_{2100}), computed as the difference in air-sea CO_2 flux relative to a control simulation with no alkalinity addition. Values are grouped according to feedstock application rate according to the low (100 g m^{-2} y^{-1}), benchmark (300 g m^{-2} y^{-1}), and high (500 g m^{-2} y^{-1}) application rate scenarios. (C), (D) Partial pressure of atmospheric CO_2 (pCO_2) over time across feedstocks for our benchmark feedstock application rate compared to a control simulation with no alkalinity addition (black).

substantial—though potentially complex—responses in surface ocean trophic structure and carbon/energy fluxes [51, 52]. The exact magnitude of these downstream ecosystem and trophic impacts will vary as a function of many factors that are not currently captured in our model, including the energetic costs of zooplankton grazing on organic-lean aggregates and differences in assimilation efficiency as a function of food quality [53, 54]. Nevertheless, our model predicts strong potential for ecosystem disruption during ocean alkalinity enhancement with natural silicate feedstocks.

The impact of synthetic alkaline metal oxides on particle composition and zooplankton ecology is potentially more muted. Dissolution of CaO in the upper ocean is sufficiently rapid that particle organic matter content and zooplankton fecal pellet production are indistinguishable from control simulations at a given ratio between feedstock application rate and net primary productivity (R_{min}; figure 2). This result is robust across a wide range of R_{min} values (see supplementary information). There is a more discernible impact of MgO on particle organic matter content and zooplankton fecal pellet production, though this scales to some extent with R_{min}. Although these impacts are relatively minor for our default PSD, a coarser distribution for MgO would be expected to have a significant impact on particle organic content (figure S15). Collectively, these results indicate that: (1) natural silicate feedstocks have minimal near-term surface alkalinity production potential but significant potential for negative impact on surface ocean ecosystems; (2) MgO (and by extension $Mg(OH)_2$) has the potential for significant near-term surface alkalinity release, but also shows complex interactions with marine particle cycling that may negatively impact surface marine ecosystems; and (3) CaO has significant near-term potential for surface alkalinity production and carbon capture from the atmosphere and may be largely benign in its impacts on particle cycling in the shallow ocean.

2.2. Carbon uptake and mitigation of ocean acidification through mineral-based ocean alkalinity enhancement

End-of-century rates of CDR during deployment of synthetic alkalinity sources amount to 5.7–20.4 Gt CO_2 y^{-1} for CaO and 6.7–23.0 Gt CO_2 y^{-1} for MgO in a moderate-emissions scenario (figure 3(A)). There is an increase in CDR rates in the high-emissions pathway because of increased efficiency of ocean carbon storage at higher background pCO_2 (figures 3(B) and (D)). Gross CDR and overall capture efficiency per unit mass of feedstock deployed are significantly lower for natural alkaline feedstocks (figures 3(A) and (B)), which exert commensurately reduced leverage on atmospheric pCO_2 (figures 3(C) and (D)). Rates of ocean CO_2 uptake for a given feedstock application rate are nearly identical for a

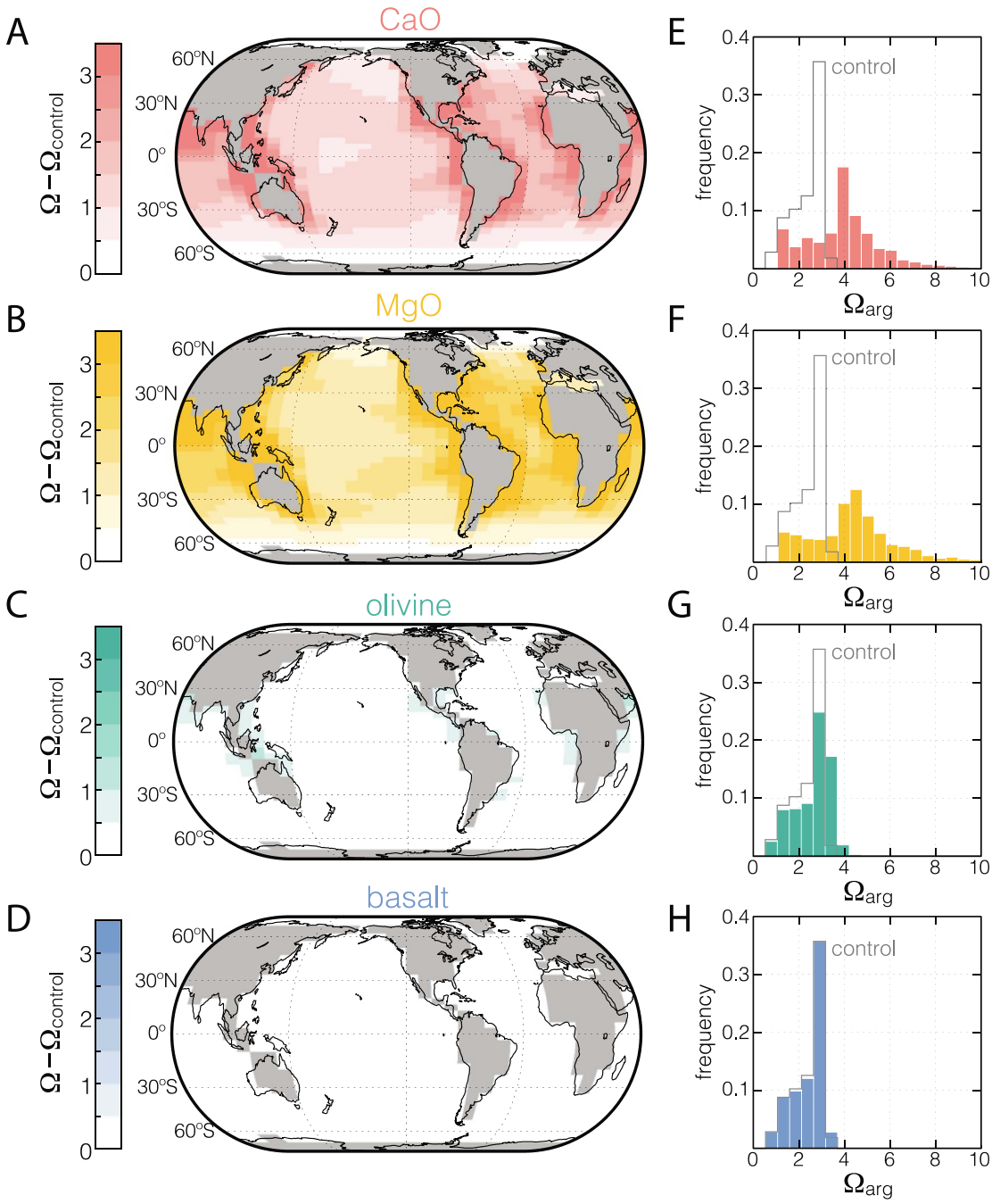

Figure 4. End-of-century (2100) carbonate saturation states during ocean alkalinity enhancement in an Earth system model. (A)–(D) *In-situ* surface ocean carbonate (aragonite) saturation states relative to a control simulation (Ω-$\Omega_{control}$) under a moderate emissions scenario (RCP4.5) with our benchmark feedstock application rate of 300 g m^{-2} y^{-1} along coastlines between 60° N/S latitude (see supplementary information). (E)–(H) Distribution of surface ocean aragonite saturation states (Ω_{arg}) from the same simulations shown in (A)–(D). Grey curve shows the distribution from the control simulation with no ocean alkalinity enhancement.

scenario in which feedstock is deployed to regions of elevated background CO_2 outgassing (see supplementary information), although regional impacts on carbonate saturation state are strongly influenced by deployment region (figure S22). Thus, different regional mitigation patterns for ocean acidification can emerge for roughly the same extent of ocean carbon capture. In any case, our results suggest that the CDR efficiency of natural alkaline feedstocks is very low, which should result in a commensurate increase in overall cost and lifecycle emissions, while the efficiency and overall potential for CDR using synthetic alkalinity sources is extremely large and is likely to be limited most directly by constraints on feedstock supply.

The ability of natural feedstocks to mitigate ocean acidification, which we proxy here by impact on surface ocean carbonate saturation states, is extremely small (figure 4). The distribution of surface ocean saturation states in our benchmark deployment

of basalt and olivine is indistinguishable from the corresponding control simulation even under a moderate anthropogenic CO_2 emissions trajectory (figures 4(C) and (D)). The impact of synthetic alkalinity sources on surface ocean carbonate chemistry is much more pronounced (figures 4(A) and (B)), with aragonite saturation states deviating significantly above those of the control simulation in our benchmark deployment of CaO and MgO (figures 4(E) and (F)). Although it will be important to fully evaluate the potential responses of marine organisms and ecosystem function to elevated carbonate saturation states [55], surface ocean saturation states in our simulated deployments of CaO and MgO should act to promote biotic calcification (e.g. [56]) while also remaining below those typically invoked to catalyze abiotic nucleation and precipitation of calcium carbonate phases [57]. This result holds across both deployment regimes considered here (figure S24).

3. Conclusions

Our results indicate first-order differences in expected ecological impact, surface ocean carbon cycling, and CDR potential across different potential feedstocks for ocean alkalinity enhancement. They also highlight major barriers that must be confronted in attempts to bring mineral-based ocean alkalinity enhancement to scale. In particular, our results indicate that application of natural silicate feedstocks (olivine and/or basalt) to surface ocean systems at rates that could conceivably result in CDR at a megaton or gigaton scale could have significant deleterious impacts on the marine biological pump and ocean trophic structure. Moving forward, directly coupled modeling of temperature feedbacks on mineral dissolution rates during transient climate simulations and explicit feedback between impacts on the biological pump, particle sinking rates, and export of carbon in the ocean interior are critical avenues for more fully evaluating the potential and impacts of deploying mineral-based ocean alkalinity enhancement at scale. It will also be critically important to obtain direct empirical constraints in field or mesocosm settings on the impacts of mineral-based alkalinity sources on particle dynamics and the potential for ecosystem disruption.

It is important to note that feedstock PSD is likely to be variable across different feedstock types, and an important topic for future research is evaluating likely PSD characteristics for different potential feedstocks along with the process CO_2 penalties and energetic demands of their production. The PSD characteristics of natural feedstocks in particular (e.g. basalt and olivine) are likely to vary substantially even within a single feedstock type [58], and the physical characteristics of synthetic alkaline metal oxide feedstocks are potentially very different from those of natural silicate mineral feedstocks. In addition, it is possible that synthetic feedstocks could be engineered to have significantly different (and more reactive) particle characteristics than natural mineral substrates, depending on the feedstock production process. Jet milling of portland cement and limestone mixtures, for instance, can produce a narrow range of very small ($\sim$4 μm) particles [59], something unlikely to be achieved for natural feedstocks without prohibitive energetic penalties. However, because our default model minimizes deleterious impacts of basalt and olivine feedstocks on particle composition and zooplankton abundance while maximizing potential alkalinity production (figure S14) we consider our primary results to be robust across a wide range of feedstock PSD scenarios.

Although alkaline metal oxides can potentially maximize near-term CDR within the ocean mixed layer and minimize the overall impact on particle compositions and zooplankton grazing, the deployment of synthetic alkalinity sources for ocean-based carbon capture at the gigaton scale may also face significant challenges. For instance, the development of novel production pathways for Mg-based feedstocks [60, 61] will likely be required to meet demand at scale. Although some CaO could be sourced from steel slag and concrete waste [46, 62], extensive deployment of limestone-derived CaO in ocean alkalinity enhancement would very likely require that calcination—the production of CaO from carbonate minerals—to be coupled to carbon capture and storage [63, 64]. In addition, the elevated reactivity of CaO may ultimately result in logistical problems during storage, transport, and application or unanticipated ecological impacts [65, 66]. In any case, our results provide strong impetus for continued techno-economic assessments of novel pathways toward alkaline metal oxide production [60] and the development of favorable life cycles for CaO and MgO deployment, along with a renewed focus on electrochemical [12, 67] and reactor-based [8] approaches toward ocean alkalinity enhancement that may be able to circumvent or minimize the potential deleterious ecological impacts and logistical barriers to scale that exist for mineral-based alkalinity sources.

Data availability statement

The data that support the findings of this study are openly available at the following URL/DOI: 10.5281/zenodo.7764796. Data will be available from 01 April 2023.

Acknowledgments

NJP acknowledges funding from the David and Lucile Packard Foundation.

Author contributions

Conceptualization: CTR, NJP, MF, ZL.
Methodology: MF, ZL, CTR, NJP.
Investigation: MF, ZL.
Visualization: MF, ZL, CTR.
Funding acquisition: CTR, NJP.
Project administration: CTR, NJP.
Supervision: CTR, NJP.
Writing—original draft: CTR, NJP, MF, ZL.
Writing—review & editing: CTR, NJP, MF, ZL.

Conflict of interest

Authors declare that they have no competing interests.

Data and materials availability

All model code and configuration files will be made available by request following publication.

References

[1] IPCC, Intergovernmental Panel on Climate Change 2018 *Global Warming of 1.5 °C An IPCC Special Report on the impacts of global warming of 1.5 °C above pre-industrial levels and related global greenhouse gas emission pathways, in the context of strengthening the global response to the threat of climate change, sustainable development, and efforts to eradicate poverty* ed V Masson-Delmonte *et al* (Cambridge: Cambridge University Press) p 616

[2] Rogelj J *et al* 2018 Scenarios toward limiting global mean temperature increase below 1.5 °C *Nat. Clim. Change* **8** 325–32

[3] van Vuuren D P *et al* 2018 Alternative pathways to the 1.5 °C target reduce the need for negative emission technologies *Nat. Clim. Change* **8** 391–7

[4] National Academies of Sciences, Engineering, and Medicine 2019 *Negative Emissions Technologies and Reliable Sequestration: A Research Agenda* (Washington, DC: The National Academies Press) (https://doi.org/10.17226/25259)

[5] National Academies of Sciences, Engineering, and Medicine 2022 *A Research Strategy for Ocean-based Carbon Dioxide Removal and Sequestration* (Washington, DC: The National Academies Press) (https://doi.org/10.17226/26278)

[6] Gruber N *et al* 2019 The oceanic sink for anthropogenic CO_2 from 1994 to 2007 *Science* **363** 1193–9

[7] Khatiwala S *et al* 2013 Global ocean storage of anthropogenic carbon *Biogeosciences* **10** 2169–91

[8] Rau G H, Knauss K G, Langer W H and Caldeira K 2007 Reducing energy-related CO_2 emissions using accelerated weathering of limestone *Energy* **32** 1471–7

[9] Renforth P and Henderson G 2017 Assessing ocean alkalinity for carbon sequestration *Rev. Geophys.* **55** 636–74

[10] Köhler P, Abrams J F, Völker C, Hauck J and Wolf-Gladrow D A 2013 Geoengineering impact of open ocean dissolution of olivine on atmospheric CO_2, surface ocean pH and marine biology *Environ. Res. Lett.* **8** 014009

[11] Kheshgi H 1995 Sequestering atmospheric carbon dioxide by increasing ocean alkalinity *Energy* **20** 915–22

[12] Rau G H 2008 Electrochemical splitting of calcium carbonate to increase solution alkalinity: implications for mitigation of carbon dioxide and ocean acidity *Environ. Sci. Technol.* **42** 8935–40

[13] Renforth P and Kruger T 2013 Coupling mineral carbonation and ocean liming *Energy Fuels* **27** 4199–207

[14] Feng E Y *et al* 2016 Could artificial ocean alkalinization protect tropical coral ecosystems from ocean acidification? *Environ. Res. Lett.* **11** 074008

[15] Feng E Y, Koeve W, Keller D P and Oschlies A 2017 Model-based assessment of the CO_2 sequestration potential of coastal ocean alkalinization *Earth's Future* **5** 1252–66

[16] Burt D J, Fröb F and Ilyina T 2021 The sensitivity of the marine carbonate system to regional ocean alkalinity enhancement *Front. Clim.* **3** 624075

[17] González M F and Ilyina T 2016 Impacts of artificial ocean alkalinization on the carbon cycle and climate in Earth system simulations *Geophys. Res. Lett.* **43** 6493–502

[18] Huack J *et al* 2016 Iron fertilization and century-scale effects of open ocean dissolution of olivine in a simulated CO_2 removal experiments *Enrivon. Res. Lett.* **11** 024007

[19] He J and Tyka M D 2022 Limits and CO_2 equilibration of near-coast alkalinity enhancement (EGUsphere)

[20] Fakhraee M, Planavsky N J and Reinhard C T 2020 The role of environmental factors in the long-term evolution of the marine biological pump *Nat. Geosci.* **13** 812–6

[21] Fakhraee M, Tarhan L G, Planavsky N J and Reinhard C T 2021 A largely invariant marine dissolved organic carbon reservoir across Earth's history *Proc. Natl Acad. Sci.* **118** e2103511118

[22] Jokulsdottir T and Archer D 2016 A stochastic, Lagrangian model of sinking biogenic aggregates in the ocean (SLAMS 1.0): model formulation, validation and sensitivity *Geosci. Model Dev.* **9** 1455–76

[23] Li X and Logan B E 1995 Size distributions and fractal properties of particles during a simulated phytoplankton bloom in a mesocosm *Deep-Sea Res.* II **42** 125–38

[24] Turner J T 2015 Zooplankton fecal pellets, marine snow, phytodetritus and the ocean's biological pump *Prog. Oceanogr.* **130** 205–48

[25] Steinberg D K and Landry M R 2017 Zooplankton and the ocean carbon cycle *Ann. Rev. Mar. Sci.* **9** 413–44

[26] Briggs N, Dall'Olmo G and Claustre H 2020 Major role of particle fragmentation in regulating biological sequestration of CO_2 by the oceans *Science* **367** 791–3

[27] Goldthwait S, Yen J, Brown J and Alldredge A 2004 Quantification of marine snow fragmentation by swimming euphausiids *Limnol. Oceanogr.* **49** 940–52

[28] Middelburg J J 1989 A simple rate model for organic matter decomposition in marine sediments *Geochim. Cosmochim. Acta* **53** 1577–81

[29] Katsev S and Crowe S A 2015 Organic carbon burial efficiencies in sediments: the power law of mineralization revisited *Geology* **43** 607–10

[30] Neikov O D, Lotsko D V and Gopienko V G 2009 Powder characterization and testing *Handbook of Non-Ferrous Metal Powders* ed O D Neikov (Oxford: Elsevier) ch 1, pp 7–44

[31] Neikov O D *et al* 2009 Mechanical crushing and grinding *Handbook of Non-Ferrous Metal Powders* ed O D Neikov (Oxford: Elsevier) ch 2, pp 47–62

[32] Beerling D J *et al* 2020 Potential for large-scale CO_2 removal via enhanced rock weathering with croplands *Nature* **583** 242–8

[33] Renforth P 2012 The potential of enhanced weathering in the UK *Int. J. Greenh. Gas Control.* **10** 229–43

[34] Cao L *et al* 2009 The role of ocean transport in the uptake of anthropogenic CO_2 *Biogeosciences* **6** 375–90

[35] Ridgwell A, Hargreaves J C, Edwards N R, Annan J D, Lenton T M, Marsh R, Yool A and Watson A 2007 Marine geochemical data assimilation in an efficient earth system model of global biogeochemical cycling *Biogeosciences* **4** 87–104

[36] Edwards N R and Marsh R 2005 Uncertainties due to transport-parameter sensitivity in an efficient 3D ocean-climate model *Clim. Dyn.* **24** 415–33

[37] Marsh R, Müller S A, Yool A and Edwards N R 2011 Incorporation of the C-GOLDSTEIN efficient climate model into the GENIE framework: "eb_go_gs" configurations of GENIE *Geosci. Model Dev.* **4** 957–92
[38] Griffies S M 1998 The gent–McWilliams skew flux *J. Phys. Oceanogr.* **28** 831–41
[39] Ridgwell A, Zondervan I, Hargreaves J C, Bijma J and Lenton T M 2007 Assessing the potential long-term increase of oceanic fossil fuel CO_2 uptake due to CO_2-calcification feedback *Biogeosciences* **4** 481–92
[40] Reinhard C T, Olson S L, Kirtland Turner S, Pälike C, Kanzaki Y and Ridgwell A 2020 Oceanic and atmospheric methane cycling in the cGENIE earth system model—release v0.9.14 *Geosci. Model Dev.* **13** 5687–706
[41] Meinshausen M *et al* 2011 The RCP greenhouse gas concentrations and their extensions from 1765 to 2300 *Clim. Change* **109** 213
[42] de Boyer Montégut C *et al* 2004 Mixed layer depth over the global ocean: an examination of profile data and a profile-based climatology *J. Geophys. Res.* **109** 426–41
[43] Economy C 2020 The circularity gap report 2020 (Circle Economy) (available at: www.circularity-gap.world/2022?gclid=CjwKCAjwitShBhA6EiwAq3RqA-FFrWmXDN8-jZIa2ZtFookxsmcfE_d6_yvOe8jB9jLdlp5enDNncxoCtqMQAvD_BwE#Download-the-report)
[44] OECD 2019 *Global Material Resources Outlook to 2060: Economic Drivers and Environmental Consequences* (Paris: OECD Publishing) (https://doi.org/10.1787/9789264307452-en)
[45] U.S. Geological Survey 2021 *Mineral Commodity Summaries* (Reston, VA: US Geological Survey) p 200
[46] Renforth P 2019 The negative emission potential of alkaline materials *Nat. Commun.* **10** 1401
[47] Cao Z, Myers R J, Lupton R C, Duan H, Sacchi R, Zhou N, Reed Miller T, Cullen J M, Ge Q and Liu G 2020 The sponge effect and carbon emission mitigation potentials of the global cement cycle *Nat. Commun.* **11** 3777
[48] Storni N, Caserini S and Grosso M 2022 The availability of limestone and other raw materials for ocean alkalinity enhancement *Glob. Biogeochem. Cycles* **36** e2021GB007246
[49] Ducklow H W, Steinberg D K and Buesseler K O 2001 Upper ocean carbon export and the biological pump *Oceanography* **14** 50–58
[50] Passow U and Carlson C A 2012 The biological pump in a high CO_2 world *Mar. Ecol. Prog. Ser.* **470** 249–71
[51] Heneghan R F, Everett J D, Blanchard J L and Richardson A J 2016 Zooplankton are not fish: improving zooplankton realism in size-spectrum models mediates energy transfer in food webs *Front. Mar. Sci.* **3** 00201
[52] Mitra A *et al* 2014 Bridging the gap between marine biogeochemical and fisheries sciences; configuring the zooplankton link *Prog. Oceanogr.* **129** 176–99
[53] Mitra A and Flynn K J 2007 Importance of interactions between food quality, quantity, and gut transit time on consumer feeding, growth, and trophic dynamics *Am. Nat.* **169** 632–46
[54] Kiørboe T 2011 How zooplankton feed: mechanisms, traits, and trade-offs *Biol. Rev.* **86** 311–39
[55] Bach L T, Gill S J, Rickaby R E M, Gore S and Renforth P 2019 CO_2 removal with enhanced weathering and ocean alkalinity enhancement: potential risks and co-benefits for marine pelagic ecosystems *Front. Clim.* **1** 00007
[56] Hoegh-Guldberg O, Poloczanska E S, Skirving W and Dove S 2017 Coral reef ecosystems under climate change and ocean acidification *Front. Mar. Sci.* **4** 00158
[57] Morse J W, ARvidson R S and Lüttge A 2007 Calcium carbonate formation and dissolution *Chem. Rev.* **107** 342–81
[58] Lewis A L *et al* 2021 Effects of mineralogy, chemistry and physical properties of basalts on carbon capture potential and plant-nutrient element release via enhanced weathering *Appl. Geochem.* **132** 105023
[59] Sun H, Hohl B, Cao Y, Handwerker C, Rushing T S, Cummins T K and Weiss J 2013 Jet mill grinding of portland cement, limestone, and fly ash: impact on particle size, hydration rate, and strength *Cem. Concr. Compos.* **44** 41–49
[60] Scott A *et al* 2021 Transformation of abundant magnesium silicate minerals for enhanced CO_2 sequestration *Nat. Commun. Earth Environ.* **2** 25
[61] Loganathan P, Naidu G and Vigneswaran S 2017 Mining valuable minerals from seawater: a critical review *Environ. Sci. Water Res. Technol.* **3** 37–53
[62] Stolaroff J K, Lowry G V and Keith D W 2005 Using CaO- and MgO-rich industrial waste streams for carbon sequestration *Energy Convers. Manage.* **46** 687–99
[63] IPCC 2005 *IPCC Special Report on Carbon Dioxide Capture and Storage. Prepared by Working Group III of the Intergovernmental Panel on Climate Change* ed B Metz *et al* (Cambridge: Cambridge University Press) p 442
[64] Renforth P, Jenkins B G and Kruger T 2013 Engineering challenges of ocean liming *Energy* **60** 442–52
[65] Glasson D R 1958 Reactivity of lime and related oxides. II. Sorption of water vapour on calcium oxide *J. Appl. Chem.* **8** 798–803
[66] Moras C A *et al* 2021 Ocean alkalinity enhancement—avoiding runaway $CaCO_3$ precipitation during quick and hydrated lime dissolution *Biogeosciences* **19** 3537–57
[67] Rau G H 2009 Electrochemical CO_2 capture and storage with hydrogen generation *Energy Proc.* **1** 823–8
[68] Rutterford L A, Simpson S D, Jennings S, Johnson M P, Blanchard J L, Schön P-J, Sims D W, Tinker J and Genner M J 2015 Future fish distributions constrained by depth in warming seas *Nat. Clim. Change* **5** 569–73